31st OptoElectronics and Communications Conference

OECC2026

June 28 (Sun) - July 2 (Thu), 2026

Paradise Hotel Busan, Busan, Korea

June 30 (Tue)	Room A	Room B	Room C	Room D	Room E	Room F	Room G	Room H	Lobby, 2F
	Grand Ballroom 1, 2F	Grand Ballroom 2, 2F	Grand Ballroom 3, 2F	Capri, 2F	Sydney, 2F	Sicily, 1F	Miami, 2F	Venice, 2F	
08:30-10:00	Tu1A	Tu1B	Tu1C	Tu1D	Tu1E	Tu1F	Tu1G		Exhibition
	Advanced Optical Technologies	Distributed Fiber -Optic Sensing II	AI-Native Autonomous Optical Access Networks	Photonic Devices in Wireless Optical Communications	Thin-Film & Reconfigurable Photonics	High-Speed Modulators II & Wavelength Conversion	Quantum Computing and Information Processing		
10:00-10:15	Coffee Break								
10:15-11:45	Tu2A	Tu2B	Tu2C	Tu2D	Tu2E	Tu2F	Tu2G		
	Optical Networks and Optical Wireless Communications	ROF & Signal Processing	Advanced Technologies for PON Evolution	Sub-THz and THz Wireless Transmission	Heterogeneous Integration for Silicon Photonics	Novel Photodetectors I	Quantum Communication and Photonic Devices		
11:45-13:15	Lunch (on your own)								
13:15-14:45	Tu3A	Tu3B	Tu3C	Tu3D	Tu3E	Tu3F	Tu3G	Industry Symposia I	
	Optical Security & Distributed Computing	Emerging Fiber-Optic Techniques	Next-Generation Access Networks	High-Symbol-Rate, High-Capacity Optical Transmission	Reconfigurable & Programmable Photonics	Novel Photodetectors II	Advanced Biomedical Imaging and Microscopy		
14:45-15:00	Coffee Break								
15:00-16:30	Tu4A	Tu4B	Tu4C	Tu4D	Tu4E	Tu4F	Tu4G	Industry Symposia II	
	AI-Native Cognitive Optical Networks	Fiber Amplifiers	Next-Generation Coherent PON	DSP for Short-Reach Optical Access	Silicon Photonics for Sensing & Imaging	III-V on Silicon Active Devices I	Computational Methods in Imaging and Microscopy		
16:30-18:00	Poster Session II (Grand Ballroom 4, 2F)								

P2-8 **16:30-18:00**

Plasmonic Lead Zirconate Titanate Phase Modulator

Liao Chen[1], Ruiji Gao[1], Jihao Zhao[1], Feng Qiu[2], Chi Zhang[1], Yang Liu[1], Xinliang Zhang[1]
[1]Wuhan National Laboratory for Optoelectronics, [2]Juhe Electro-Optic Tech. Co. Ltd.

We demonstrate an efficient plasmonic lead zirconate titanate phase modulator. The proposed plasmonic modulator achieves a modulation efficiency of 996 V·μm and a 6-dB electro-optic bandwidth exceeding 65 GHz.

P2-9 **16:30-18:00**

Fabrication of a DBR Resonator Based on Nb_2O_5 Horizontal Slot Waveguides with a 100-nm-Thick Hollow Slot for Sensing Devices

Katsumi Nakatsuhara, Umi Endo, Nao Suzuki, Yoshiki Hayama
Kanagawa Institute of Technology

We designed and fabricated DBR resonators based on Nb2O5 horizontal slot waveguides with 100-nm-thick hollow slots. Furthermore, refractive-index changes were observed in the fabricated devices.

P2-10 **16:30-18:00**

Quantitative Characterization of Nonlinear Resonance Shifts in Silicon Microrings Using Multi-FSR Probe Characterization

Chia-Chien Wei, Shou-Ting Peng, Huei-Hua Lai, Yung-Jr Hung
National Sun Yat-sen University

We experimentally demonstrate the true resonance shifts of silicon microrings under high-power injection using multiFSR characterization. This method eliminates nonlinear artifacts, enabling the first experimental reconstruction of intrinsic, steady-state spectral profiles.

P2-11 **16:30-18:00**

Time-Domain Interleaving Model for Nonlinear Dynamics in Silicon Micro-Ring Modulators

Zhiyuan Zhou[1,3], Zhihan Sun[1,3], Yueyang Yu[1,3], Yu Lu[1,3], Qingyun Xian[1,3], Qi Tian[1,3], Changyu Hu[2], Hao Hu[2], Jun Liu[2], Shengjiang Dai[2], Shuang Zheng[1,3,4], Minming Zhang[1,3,4]
[1]Huazhong University of Science and Technology, [2]Hubei Jiufengshan Laboratory, [3]National Engineering Research Center for Next Generation Internet Access System, [4]Optics Valley Laboratory

We propose a time-domain interleaving model for silicon micro-ring modulators capturing thermal and free-carrier nonlinearities. Validated by experiments, the model accurately simulates sweep-speed-dependent spectra and insertion-loss-dependent bandwidths, while predicting selfpulsation dynamics.

P2-12 **16:30-18:00**

A 36 Gb/s Silicon Micro-Ring Modulator Transmitter with Driver Resistance Optimized for Bonding-Wire Inductance

Sehwan Park[1], Dae-Won Rho[2], Yongjin Ji[1], Jaewon Lee[1], Woo-Young Choi[1]
[1]Yonsei University, [2]Texas A&M University

This paper presents a silicon (Si) micro-ring modulator (MRM) transmitter with package-level optimization of the driver resistance considering bonding-wire inductance. The implemented MRM transmitter achieves 36 Gb/s PRBS-31 NRZ operation with 3.87 pJ/bit energy efficiency.

P2-13 **16:30-18:00**

SiN 2 × 2 Mach-Zehnder Thermo-Optic Switch with P_π < 40 mW and Response Time < 30 μs

Yuanhao Li, Haojie Xue, Luyang Liu, Yichen Zhang, Lei Zhang
Beijing University of Posts and Telecommunications

We report a 2 × 2 SiN thermo-optic switch with folded Euler-spiral phase shifter. At 1550 nm, it achieves ~ 38 mW P_π, > 50 dB cross-port extinction ratio, < 30 μs switching.

P2-14 **16:30-18:00**

Resonance-Enhanced Coherence Network for an On-Chip IR Computational Spectrometer

Zhijie Wei, Zunyue Zhang, Rui Niu, Tiegen Liu, Zhenzhou Cheng
Tianjin University

We investigate an on-chip infrared computational spectrometer based on a resonance-enhanced coherence network, aiming to enhance spectral diversity by jointly magnifying structural dispersion and effective optical path difference.

A 36 Gb/s Silicon Micro-Ring Modulator Transmitter with Driver Resistance Optimized for Bonding-Wire Inductance

Sehwan Park*, Dae-Won Rho**, Yongjin Ji*, Jaewon Lee*, and Woo-Young Choi *
* Department of Electrical and Electronic Engineering, Yonsei University, Seoul, Republic of Korea
** Formerly at Yonsei University when this work was done. Now at Texas A&M University, College Station, TX, USA

Abstract

This paper presents a silicon (Si) micro-ring modulator (MRM) transmitter with package-level optimization of the driver resistance considering bonding-wire inductance. The implemented MRM transmitter achieves 36 Gb/s PRBS-31 NRZ operation with 3.87 pJ/bit energy efficiency.

I. Introduction

The MRM is a key element in high-performance optical interconnect solutions for artificial intelligence (AI) and machine learning (ML) computing applications [1]. Although various analyses of MRMs have been reported [2], [3], the effect of bonding-wire inductance has not been fully addressed. In this work, the effect of bonding-wire inductance between the electronic IC (EIC) driver and the MRM is investigated using an equivalent circuit, and the EIC driver resistance is optimized accordingly.

II. Package-Level Analysis and EIC Driver Optimization

Bonding wires introduce parasitic inductance between the EIC driver and the MRM, which can significantly affect the high-speed modulation response. Fig. 1 shows the simulated 36 Gb/s eye diagrams at the MRM optical output, obtained using an ideal input signal applied to the EIC driver. The MRM is modeled using a large-signal piecewise-linear circuit model [4]. Fig. 1(a) shows a clear eye opening in the absence of bonding-wire inductance, whereas Fig. 1(b) shows a degraded eye diagram when bonding-wire inductance is included. This result clearly indicates that bonding-wire inductance must be considered in the design of high-speed MRM transmitters.

Fig. 2 shows the package-level equivalent circuit of the EIC driver and the MRM connected by bonding wires. Here, V_{predrv} denotes the input voltage of the EIC driver, R_{drv} represents the output resistance of the EIC driver, and C_{tot} is the sum of the parasitic capacitance at the EIC driver output node and the pad capacitance. In addition, L_{wire} denotes the inductance of the bonding wire, while C_{pad} represents the parasitic capacitance formed by the MRM pad and the metal interconnect line.

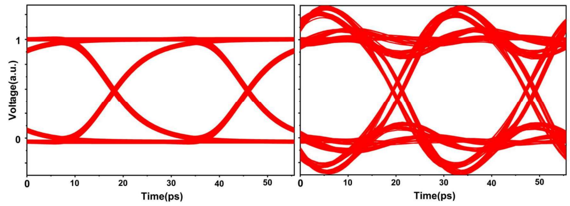

(a) (b)

Fig. 1. Simulated 36 Gb/s eye diagrams at the MRM output: (a) without bonding-wire inductance and (b) with bonding-wire inductance.

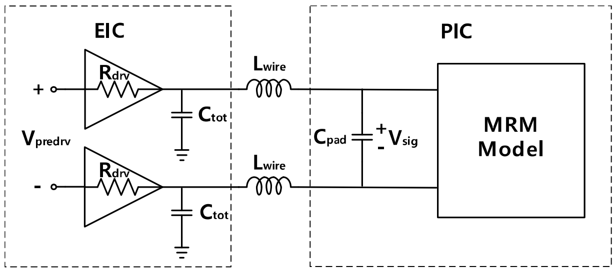

Fig. 2. Equivalent circuit of the EIC driver and the photonic IC (PIC) MRM connected by bonding-wires.

The transfer function of the equivalent circuit is given as

$$\Delta H(s) = \frac{V_{sig}(s)}{V_{predrv}(s)}$$

$$= \frac{1}{R_{drv}L_{wire}C_{tot}C_{pad}} \cdot \frac{1}{s + \frac{1}{R_{drv}C_{tot}}} \cdot \frac{1}{s^2 + \frac{1}{2L_{wire}C_{pad}}}. \quad (1)$$

The term $1/(s^2 + 1/2L_{wire}C_{pad})$ represents the LC resonant component formed by L_{wire} and C_{pad}, which induces peaking at the natural frequency $\omega_n = \sqrt{1/(2L_{wire}C_{pad})}$. However, the term $1/(s + 1/R_{drv}C_{tot})$ suppresses the high-frequency response, alleviating the resonance-induced peaking. Accordingly, for a given L_{wire}, R_{drv} can be selected to provide sufficient bandwidth (BW) at the target data rate without excessive peaking.

This work was supported by the Institute of Information & Communications Technology Planning & Evaluation (IITP) grants funded by the Korea government (MSIT) (No. RS-2023-00222171, No. RS-2025-02304291).

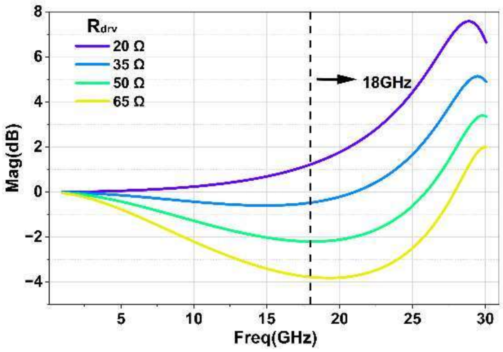

Fig. 3. Simulated frequency responses for different R_{drv} values at L_{wire} = 1 nH.

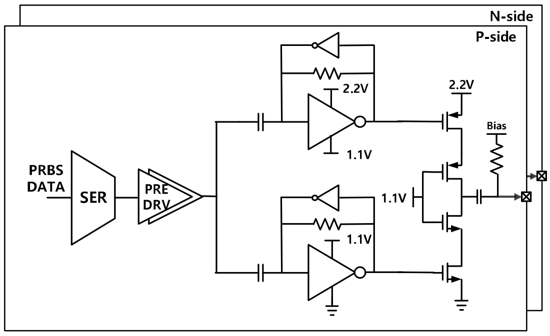

Fig. 4. Architecture of the EIC driver.

Fig. 3 shows the simulated frequency responses for different R_{drv} values at L_{wire} = 1 nH, which corresponds to the calculated inductance of the approximately 1100 µm bonding wire used in our package. When R_{drv} = 20 Ω, peaking is not sufficiently suppressed at the Nyquist frequency of 18 GHz. As R_{drv} increases, the peaking is reduced. However, large R_{drv} can reduce the magnitude at the Nyquist frequency. Based on the simulated results, R_{drv} = 35 Ω is identified as the optimal value considering both peaking suppression and the magnitude at the Nyquist frequency.

Fig. 4 shows the architecture of the EIC driver. To obtain a sufficiently large optical modulation amplitude (OMA), a differential voltage swing of 4.4 V is applied to the MRM. Accordingly, the serialized data are divided into two paths: a 0 V to 1.1 V data path and a level-shifted 1.1 V to 2.2 V data path, which are then applied to the EIC driver. In addition, to provide a reverse bias across the MRM, the output of the P-side EIC driver is biased at 1.1 V, while the N-side is biased at 3.3 V.

III. Measurement Results

Fig. 5(a) shows the chip micrograph of the implemented MRM transmitter. The EIC is fabricated in Samsung 28-nm CMOS, while the MRM is fabricated in the AMF Si photonics foundry. Fig. 5(b) shows the measured 36 Gb/s eye diagram at the MRM output. For the measurement, a PRBS-31 signal with a differential swing of 4.4 V_{pp} is applied to drive the MRM. The measurement setup consists of a Keysight MSOV334A oscilloscope,

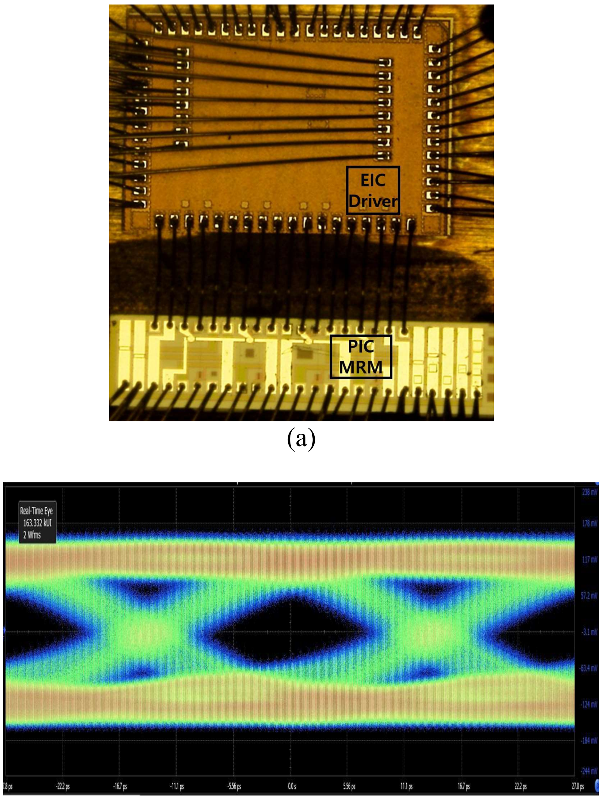

(a)

(b)

Fig. 5. (a) Chip micrograph. (b) Measured 36 Gb/s PRBS-31 NRZ eye diagram at the MRM output.

an Agiltron EDFA, a Coherent XPDV2320R photodetector with 50 GHz BW and a Quantifi Photonics tunable laser source operating at 1550 nm. At the data rate of 36 Gb/s, the MRM transmitter achieves an energy efficiency of 3.87 pJ/bit.

IV. Conclusions

We demonstrate a 36 Gb/s PRBS-31 NRZ MRM transmitter in which the EIC driver resistance is optimized considering bonding-wire inductance. The implemented MRM transmitter achieves an energy efficiency of 3.87 pJ/bit.

Acknowledgment

The chip fabrication was supported by the Samsung Electronics and the EDA tool was supported by the IC Design Education Center (IDEC), Korea.

References

[1] C. Xie et al., “Scaling optical interconnects for hyperscale data center networks,” in Proceedings of the IEEE, vol.110, no.11, pp. 1699–1713, Nov. 2022.

[2] J. Rhim et al., "Verilog-A behavioral model for resonance-modulated silicon micro-ring modulator," Optics Express, vol. 23, no. 7, pp. 8762–8772, Mar. 2015.

[3] M. Shin et al., "A Linear Equivalent Circuit Model for Depletion-Type Silicon Microring Modulators," in IEEE Transactions on Electron Devices, vol. 64, no. 3, pp. 1140-1145, March 2017.

[4] M. Kim et al., "Large-signal SPICE model for depletion-type silicon ring modulators," Photonic Research, vol.7, no.9, p.948, Sep. 2019.